The Influence of Airflow transport Path on Precipitation during the Rainy Season in the Liupan Mountains of Northwest China

Yujun Qiu[1*], Chunsong Lu [1], zhiliang Shu [2,3] , Peiyun Deng [2,3]

[1] *Key Laboratory of Aerosol-Cloud-Precipitation of China Meteorological Administration, Nanjing University of Information Science & Technology, Nanjing*, 210044, *China*

[2] *Key Laboratory for Meteorological Disaster Monitoring and Early Warning and Risk Management of Characteristic Agriculture in Arid Regions, China Meteorological Administration, Yinchuan*, 750002, *China*

[3] *Ningxia Key Laboratory of Meteorological Disaster Prevention and Reduction, Yinchuan*, 750002, *China*

ABSTRACT

Utilizing observational data from seven ground gradient stations located on the eastern slope, western slope, and mountaintop of Liupan Mountains (LM) during the rainy seasons from 2020 to 2022, combined with backward trajectory cluster analysis, this study investigated the influence of airflow transport paths on the seasonal rainfall in this mountainous region. The results indicate: (1) LM's rainy season, characterized by overcast and rainy days, is mainly influenced by cold and moist airflows (CMA) from the westerly direction and warm and moist airflows (WMA) from a slightly southern direction. The precipitation amounts under four airflow transport paths are ranked from largest to smallest as follows: WMA, CMA, warm dry airflows (WDA), and cold dry airflows (CDA). (2) WMA contribute significantly more to the intensity of regional precipitation than the other three types of airflows. During localized precipitation events, warm airflows have higher precipitation intensities at night than cold airflows, while the opposite is true during the afternoon. (3) During regional precipitation events, water vapor content is a primary influencing factor. Precipitation characteristics under humid airflows are mainly affected by high water vapor content, whereas during dry airflow precipitation, dynamic and thermodynamic factors have a more pronounced impact than for humid airflows. (4) During localized precipitation events, the influence of dynamic and thermodynamic factors is more complex than during regional precipitation, with precipitation characteristics of the four airflows closely related to their water vapor content, air temperature and humidity attributes, and orographic lifting. (5) Compared to regional precipitation, the influence of topography is more prominent in localized precipitation processes.

Key words: Regional precipitation, Localized precipitation, Airflow transport, Water vapor flux, Instability energy, Topographic influence

https://doi.org/10.1007/s00376-024-3162-6

Article Highlights:

- The precipitation amounts under the influence of WMA, CMA, WDA, and CDA air flows in the LM rainy season account for 68%, 12%, 10%, and 9.8% of the total precipitation, respectively.
- The regional precipitation intensity generated by WMA is greater than that of the other three types of airflows, exhibiting characteristics of high water vapor flux and low instability energy.
- During the regional precipitation process, dynamic and thermodynamic factors are notably evident in the precipitation of dry airflows, with CDA demonstrating the most significant manifestation in strong nighttime precipitation events.
- Under the influence of topography, the dynamic and thermodynamic factors have a more significant impact on localized precipitation than on regional precipitation.

1 Introduction

The water vapor resources for heavy rainfall in China during summer are primarily influenced by the southwesterly water vapor transport from the Bay of Bengal and the South China Sea (Tao and Chen, 1987; Simmonds et al., 1999; Zhou and Yu, 2005; Huang et al., 2017). For one of the regions with the scarcest water resources in China, the northwest area, its water vapor transport mainly relies on two circulation systems: the monsoon and the westerlies (Feng and Zhou, 2012; Li et al., 2015; Li et al., 2016; Wang et al., 2018; Xu et al., 2020). However, as of now, there are few reports on the exact impact that airflows of different directions and characteristics have on precipitation in this region.

Many studies have indicated that the efficiency of water vapor conversion to precipitation is low in this region (Wang et al., 2005; Cheng et al., 2006; Wang et al., 2016; Zhang et al., 2020). Other research has pointed out that the aerial water resources in this area mainly follow the distribution along mountainous regions (Chen et al., 2005; Liu et al., 2018; Zhang et al., 2020; Qi et al., 2022), suggesting that both different characteristics of air mass transport and mountainous terrain play significant roles in precipitation in the region. It is necessary to connect the two to study the characteristics of regional precipitation. Compared with other major mountain ranges in the northwest region, Liupan Mountains (LM) are situated against the complex terrain backdrop of the eastern edges of the Tibetan Plateau and the northwestern edges of the Loess Plateau. Here, a higher proportion of hydrometeors remains untransformed into precipitation (Zhang et al., 2020). Studying the precipitation characteristics under different air mass transport pathways in this region will have important implications for regional rain enhancement, drought resistance, and ecological and environmental protection.

Under the influence of favorable weather systems, mountainous terrain significantly alters the dynamic and thermodynamic characteristics of moisture transport through convergence and orographic lifting, thereby affecting regional clouds and precipitation weather (Banta, 1990; Barros et al., 1994; Neiman et al., 2002; Seity et al., 2003; Houze and Medina, 2005; Giovannettone and Barros, 2009; Houze, 2012). There is also a notable difference in cloud water resources and precipitation weather between the windward and leeward slopes (Sevruk and Neveni, 1998; Scholl et al., 2007; Houze, 2012; Gao, 2020; Deng et al., 2021; Xu et al., 2023). Many studies have focused on the impact of the Qilian Mountains (QM) terrain, located on the northwest side of the LM, on cloud water resources. They pinpoint that orographic uplift has a crucial effect on the intensity of stratocumulus precipitation and the amount of cloud coverage. The annual precipitation is closely related to stratiform clouds and summertime cumulus clouds, with the distribution of atmospheric moisture and precipitation being closely linked to elevation, slope aspect, and circulation (Zhang et al., 2008; Wang et al., 2018; Gui et al., 2022; Qi et al., 2022).

Compared to the QM, the LM are situated in the southeastern part of the northwest region and are comparatively smaller in scale, yet have an annual precipitation amount close to that of the QM (Zhang et al., 2020). Gao (2020) conducted a study using 30 years of daily precipitation data from six national meteorological stations in the LM region, indicating that the precipitation on the eastern side is more than that on the western side. Deng et al. (2021) used 30-year reanalysis data from the European Centre for Medium-Range Weather Forecasts (ECMWF) along with meteorological station precipitation observations, pointing out that the eastern side of the LM exhibits higher amounts of precipitable water in the atmosphere, water vapor flux, specific humidity, and actual precipitation compared to the western side. Xu et al. (2023) identified that both the cloud water content and precipitation of the LM decrease gradually from south to north along a southwestward latitude, with the eastern side having 15% and 18% more, respectively, than the western side. The studies suggest that the interplay between upper and lower level weather systems, combined with the barrier effect of the LM, are the primary reasons for the higher precipitation amounts and atmospheric water vapor on the eastern slopes compared to the western slopes.

Based on the current state of research and considering the close relationship between mountain precipitation and factors such as elevation, slope aspect, and circulation, this paper utilizes three consecutive years of observational data from gradient stations on the eastern and western slopes of the LM. Combined with cluster analysis using the Hybrid Single-Particle Lagrangian Integrated Trajectory (HYSPLIT) model, this study meticulously analyzes the precipitation characteristics under the influence of airflows with different attributes. The results of this research have significant scientific guidance for the development and utilization of precipitation resources in the LM, as well as for aspects like anthropogenic operations.

2. Data and methodology

2.1 Study area introduction

LM is located on the edge of the Asian monsoon influence zone, situated in the southern part of the Ningxia Hui Autonomous Region in China. It is one of the few continuous mountain ranges in the country with an approximate north-south orientation (at an angle of about 30 degrees). The regional range is between 34.7-36.5°N latitude and 105.2-107°E longitude. The mountain ridge exceeds an altitude of 2500 meters, with the highest peak reaching 2942 meters, and the lowest point at 1599 meters. The western slope of the mountain body is gentle, while the eastern slope is steep, with the southwest being the predominant slope direction (See Figure 1).

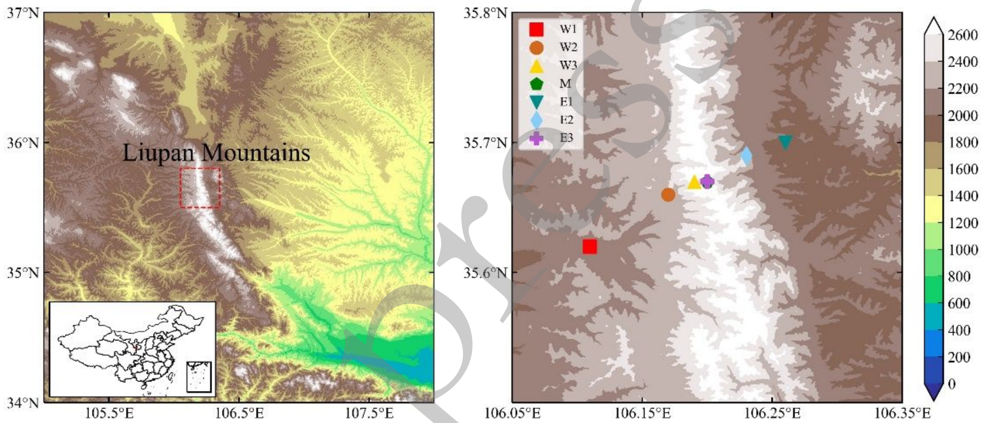

Figure 1: Geographical location and terrain of the LM, and the distribution of seven observation sites. The sites located on the western slope, with elevations increasing from low to high, are W1, W2, and W3. The sites on the eastern slope, also with elevations increasing from low to high, are E1, E2, and E3. The site at the mountain's peak is labeled as M. Among them, E3 and M are close in latitude and longitude, with an altitude difference of 220 meters.

2.2 Data Description

Since September 2019, meteorological observation stations have been established at six different altitudes on the east and west slopes of the research area. The stations on the west slope are arranged in ascending order of altitude and are sequentially denoted as W1, W2, and W3. Corresponding to the heights of the west slope stations, the east slope stations are denoted as E1, E2, and E3, respectively. In addition, there is the highest-altitude summit station M, which is a national benchmark climate station. These seven stations are collectively referred to as ground gradient stations. The latitude, longitude, and elevation details of each station are presented in Table 1.

Table 1: Latitude, Longitude, and Elevation of the Seven Ground Observation Stations in the LM

Station	name	Longititude(°)	Latitude(°)	Altitude（km）
W1	Fengtailinchang	106.11°	35.62°	2.223
W2	Yangjiadian	106.17°	35.66°	2.323
W3	Liupanshan	106.19°	35.67°	2.599
M	NRCS	106.20°	35.67°	2.822
E1	Dawansubao	106.26°	35.70°	1.957
E2	Liupanshan Town	106.23°	35.69°	2.347
E3	Heshangpuling	106.20°	35.67°	2.602

The ground gradient stations have accumulated three years of observational data since their establishment. This paper utilizes atmospheric pressure, temperature, wind speed, relative humidity, and hourly precipitation data observed from July to September of each year from 2020 to 2022.

Additionally, the Global Data Assimilation System (GDAS) data released by the National Centers for Environmental Prediction (NCEP) in the United States was also employed to analyze the pathways of air mass transport. The timing of this data is consistent with the observational records from the ground gradient stations.

This study also utilized precipitation data from the 5th generation global atmospheric reanalysis (ERA5), released by the European Centre for Medium-Range Weather Forecasts (ECMWF). The data covers a period of 33 years, from January 1, 1990, to December 31, 2022, to provide a regional average level of precipitation for the LM area.

2.3 Methodology

2.3.1 Selection of the rainy season

The precipitation trend of the seven ground gradient stations in the LM from July to September during 2020-2022 is consistent with the ERA5 precipitation trend (see Figure 2a). The average observed ground precipitation is only 5.2% higher than the ERA5 precipitation values, indicating the ERA5 data reflect the precipitation capacity of the LM accurately. Consequently, this study utilizes ERA5 precipitation data to select the months of the rainy season for the LM. The total precipitation from July to September in the LM region accounts for 52% of the annual total precipitation (see Figure 2b). A study by Gao (2020) also used nearly 30 years of daily precipitation data from six national meteorological stations in the LM area, noting that precipitation is mainly concentrated between July and September, accounting for 50%-60% of the annual total. Therefore, this paper identifies July to September as the representative months for the rainy season in this region.

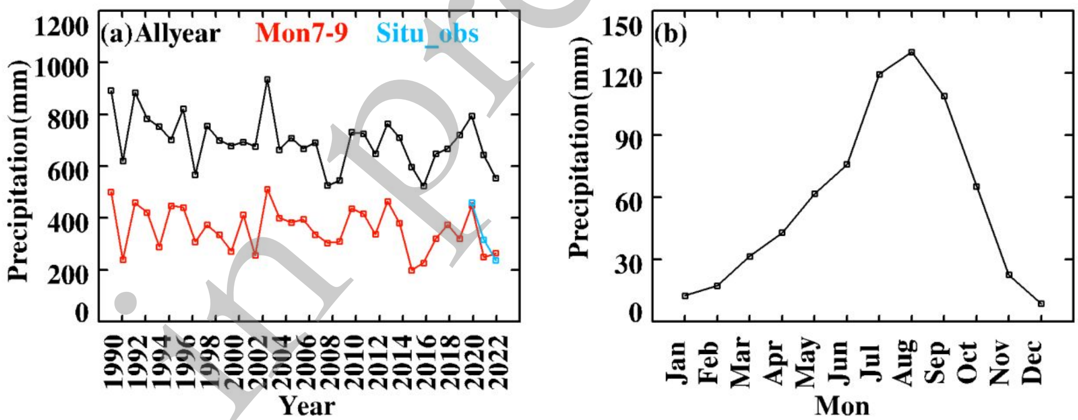

Figure 2: Precipitation in the LM region based on ERA5 from 1990 to 2022, (a) annual total precipitation series, (b) monthly total precipitation series for 1-12 months. In (a), the black dotted line represents the total precipitation for each month of the year, the red dotted line represents the total precipitation for July to September each year, and the blue dotted line represents the mean total precipitation for July to September at the 7 ground gradient stations.

2.3.2 Water vapor flux and instability energy

Water vapor flux (Wv) refers to the amount of water vapor transported through a unit area in a unit time and can characterize the strength of water vapor transport. In this study, we have calculated the Wq within the vertical atmospheric column between adjacent stations on either the west or east slope using data observed at ground gradient sites, with the calculation method described in equation (1).

$$W_v = -\frac{1}{g}\int_{p_1}^{p_2} vq\,dp \qquad (1)$$

The unit for Wv is mm/min. Here, ‘g’ stands for gravitational acceleration, ‘q’ represents specific humidity, ‘p’ denotes atmospheric pressure, ‘p1’ is the pressure at Site 1, and ‘p2’ is the pressure at Site 2, which is adjacent to and higher than Site 1, with the unit in hPa. The term ‘v’ signifies the wind speed at the site, with the unit in m/s.

The unstable energy (Ue) refers to the energy within an atmospheric layer that can cause a unit mass air parcel to rise. In this paper, we have calculated the Ue for a unit mass air parcel ascending from the isobaric surface at pressure p1 at Site 1 to the isobaric surface at pressure p2 at Site 2. The calculation method is shown in equation (2).

$$U_e = R_d\int_{p_1}^{p_2}(T_v - T_{ve})\,d(-\ln P) \qquad (2)$$

The unit of Ue is J/kg·m. Rd represents the specific gas constant for dry air and is 287.0 J/K·kg. Tv is the virtual temperature of the rising air parcel, and Tve is the virtual temperature of the surrounding environment of the rising air parcel. The difference between Tv and Tve is approximated using the difference between the site temperature and the environmental air temperature assuming a dry adiabatic lapse rate.

2.3.3 Classification of Airflow Transport Pathways

In this paper, we have used the backward trajectory clustering method of HYSPLIT (Hybrid Single-Particle Lagrangian Integrated Trajectory Model) to categorize the moisture transport pathways over LM from July to September for the years 2020 to 2022. This method, jointly developed by the National Oceanic and Atmospheric Administration (NOAA) and other agencies, is a model capable of handling different meteorological element inputs and tracing the origins of airflows. Referring to the summit station as the reference location, the angle method is employed to group a large number of trajectories according to the closest angle principle after conducting a 24-hour backward tracking of the transport airflows at the 3km height layer. The HYSPLIT model uses data from the NCEP Global Data Assimilation System (GDAS).

3. Results and Analysis

3.1 Types of transporting airflow and characteristics of precipitation

LM is located in the northwest of China and is significantly influenced by the mid-latitude westerly belt. In summer, the zonal moisture transport is more pronounced compared to the meridional transport (Huang and Chen, 2010). Figure 3, obtained from the backward trajectory clustering, reflects this transport characteristic through eight distinct air mass transport pathways. From pathway 3 (Pth3) to pathway 5 (Pth5), these three pathways are all within the range of zonal moisture transport and together account for 50.4% of the total air mass transport pathways. Pathways Pth6 to Pth8 lie within the range influenced by the oblique southerly monsoon transport and together constitute 31.8% of the total transport pathways.

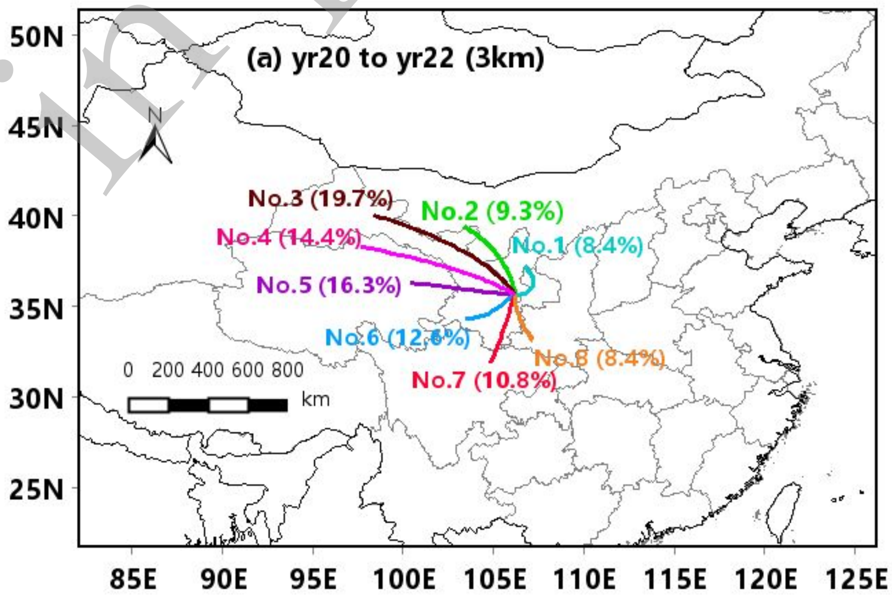

Figure 3: Clustering of airflow transport trajectories and the percentage at a height of about 200m above the mountaintop (3km above sea level) with the mountaintop station as the reference position during the rainy season (July-September) from 2020 to 2022.

Comparing the precipitation amounts under different air mass transport pathways (as shown in Figure 4b), it is observed that the annual average precipitation and cumulative precipitation duration at the site under different air mass transport pathways are not correlated with the percentage numbers of the airflow transport pathways. The majority of the precipitation during the rainy season in LM is concentrated along pathways Pth6- Pth8, accounting for 68.3% of the total precipitation. As depicted in Figure 3, the directions of these three air mass transport pathways point towards the Indian Ocean and the South China Sea, which is associated with the monsoonal moisture transport in a warm and humid environment. In terms of cumulative precipitation duration, the zonal transport pathway Pth5 is also significant. The duration of precipitation under this pathway is comparable to the meridional transport pathway Pth7, but the former has a significantly lower amount of precipitation, only 54% of the latter.

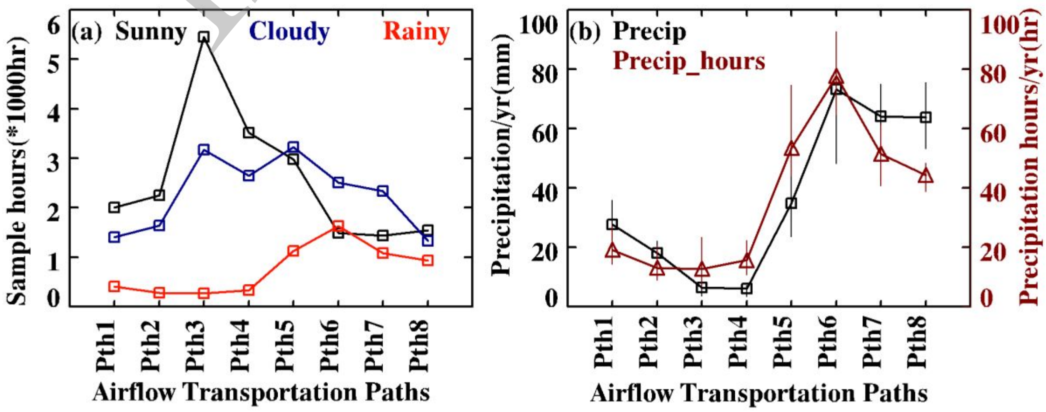

Figure 4: Comparisons in different airflow transport paths in LM from 2020 to 2022 during July

to September, (a) cumulative hours of clear days/cloudy days/precipitation (b) annual average precipitation and cumulative precipitation hours.

To further investigate the reasons for the precipitation differences under different air mass transport pathways, a comparison was made for wind speed, temperature, and specific humidity under conditions of clear skies (relative humidity < 80%, precipitation amount 0 mm), overcast skies (relative humidity ⩾ 80%, precipitation amount 0 mm), and rainy conditions (precipitation amount > 0 mm) for each pathway, with the results shown in Figures 5a-5c. Compared to overcast and rainy conditions, the conditions for each pathway under clear skies show higher wind speeds, higher temperatures, and lower specific humidity. To enable a direct numerical comparison of different pathways and meteorological elements, the values for wind speed, temperature, and specific humidity were standardized (ranging between 0 and 1), resulting in a standardized index (SI) for each meteorological element. By adding the wind speed SI, temperature SI, and specific humidity SI for each pathway, a Meteorological Standardized Index (MSI) corresponding to each pathway is obtained, as shown in Figure 5d.

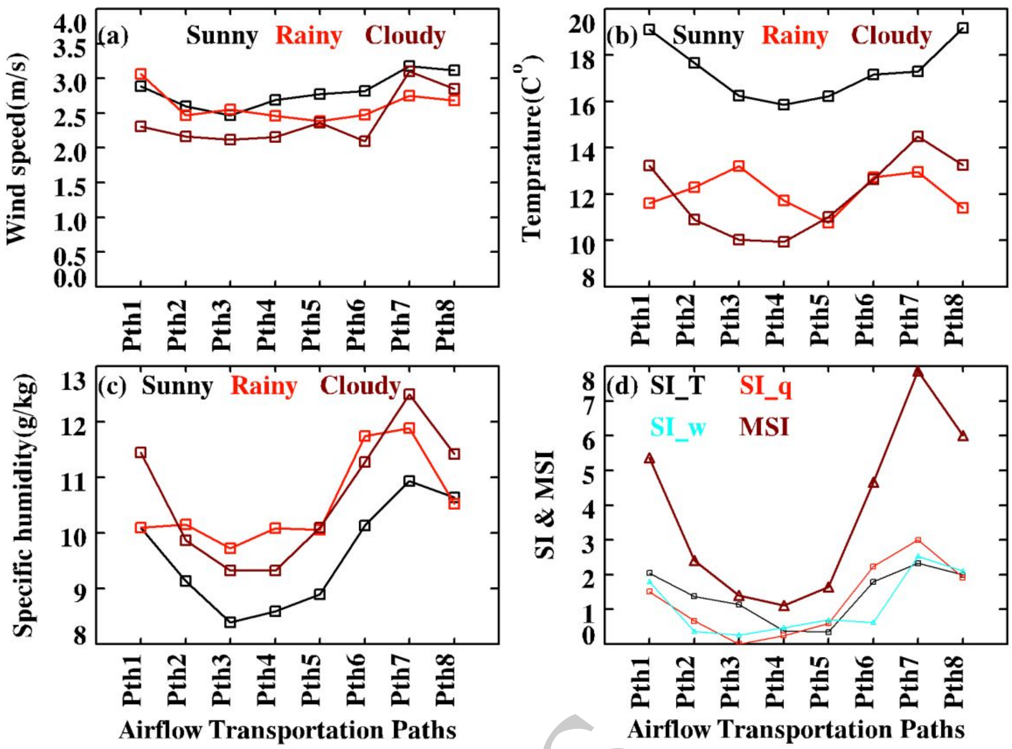

Figure 5: Comparisons of the wind speed, temperature, specific humidity, standardized index (SI), and meteorological standardized index (MSI) of the eight airflow transport paths in the LM during the rainy season (July-September) from 2020 to 2022 under precipitation, cloud, and clear sky conditions. (a) Wind Speed, (b) Temperature, (c) Specific Humidity, (d) Standardized Index (SI) and Meteorological Standardized Index (MSI)

From Figure 5d, it can be seen that the Meteorological Standardized Index (MSI) for Pth1, Pth6-Pth8 is significantly higher than that of the other pathways. This does not entirely coincide with the distribution of the precipitation values across the pathways. In an effort to further understand the reasons behind this, a comparison was made of the wind speed SI, temperature SI, specific humidity SI, and MSI values across the pathways (as shown in Table 2). The temperature SI is used to determine the thermal characteristics of the airflow; a pathway's airflow is classified as warm when its temperature SI is higher than the average value of all pathways, and as cold when a pathway's temperature SI is below the average. Within the warm airflows, Pth1 and Pth6-8 exhibit differences; the former has a temperature SI greater than humidity SI, whereas for the latter, it is the opposite. To distinguish between these two situations, Pth1 is characterized as a warm-dry airflow（WDA）, and Pth6-8 as a warm-moist airflow（WMA）. Similarly, among the cold airflows, Pth2-4 and Pth5 have different characteristics; the former has a temperature SI greater than humidity SI, and for the latter, the opposite is true, leading to Pth2-4 being characterized as a cold-dry airflow（CDA）, and Pth5 as a cold-moist airflow（CMA）.

Table 2 Comparisons of SI of different meteorological elements, MSI, and warm/cold-dry/humid properties of airflow on different transport paths in the LM during July-September from 2020 to 2022. The suffix '_Wd', '_T' and '_Hd' represent the wind speed, temperature and humidity, respectively.

Transport path（Tr）	Wind speed SI_W	Temprature SI_T	Humidity SI_H	MSI characterization	Warm/cold/moist /dry properties
Tr 1	＞ave.	＞ave.	＞ave.	Large SI_W, SI_T＞SI_H, large MSI	Warm-dry
Tr 2-4	＜ave.	＜ave.	＜ave.	;Little SI_W, SI_T＞SI_H, little MSI	Cold-dry
Tr 5	＜ave.	＜ave.	＜ave.	Little SI_W, SI_T＜SI_H, little MSI	Cold-moist
Tr 6	＜ave.	＞ave.	＞ave.	Little SI_W, SI_T＜SI_H, large MSI	Warm-moist
Tr 7-8	＞ave.	＞ave.	＞ave.	Large SI_W, SI_T≤SI_H, large MSI	Warm-moist

A comparison of the cumulative hours of clear and overcast rainy weather under each air mass transport pathway (as detailed in Figure 4a) reveals that the pathways characterized by WMA and CMA (Pth5-Pth8) experience more overcast rainy hours than clear hours, with the former being 1.9 times that of the latter, and accounting for 80.2% of the total pathway precipitation. Pathways with WDA and CDA (Pth1-Pth4) exhibit more clear weather hours than overcast rainy hours, with the former being 1.3 times that of the latter. The characteristics of the cumulative overcast rainy hours along these air mass transport pathways are closely related to the distribution of precipitation, as seen in Figures 4b and 5d. The amount of precipitation along the air mass transport pathways is closely related to the warm-moist attributes of the airflow, with the precipitation pattern distributed in the following order: WMA >CMA> WDA> CDA.

Feng and Zhou (2012) investigated the sources of water vapor transport in the large geomorphology located southwest of the LM - the southeastern part of the Tibetan Plateau. They noted that the main sources of water vapor transport in this region are the Indian summer monsoon from the Arabian Sea and the Bay of Bengal. The transport direction of the WMA (Western Moisture Area) points towards the Indian Ocean, the Bay of Bengal, and southeast. Precipitation along these paths is often closely related to warm and moist airflows from a more southerly direction. Meanwhile, the CMA points towards the zonal flow of the westerlies. During the airflow transport process, the air mass is lifted by the terrain as it passes over the Tibetan Plateau, and subsides over the low-level moist air of the rainy season when it crosses the region, converging with the low-level terrain uplift airflow of the LM area to facilitate precipitation. Although the WDA (Western Dry Area) accounts for a smaller proportion of the total transport path, the precipitation amount is comparable to that of the CDA (Central Dry Area). The airflow for WDA is transported from the northwest to the eastern side of the LM, where it is deflected northeastward due to obstruction by the terrain of QM remnants.

3.2 Precipitation intensity characteristics

Based on precipitation data from observation sites, it has been found that single precipitation events can last from just 1 hour of brief rainfall to more than 48 hours of continuous rain events. Typically, regional precipitation caused by large-scale weather systems has a longer duration and wider coverage. In contrast, localized precipitation, influenced by topography and local dynamic and thermodynamic effects, occurs within specific periods and tends to have a shorter duration and smaller coverage. We differentiated between these two types of precipitation using the following criteria: instances where precipitation occurred at all 7 stations, and at least 4 stations experienced precipitation lasting more than 6 hours, were classified as regional precipitation samples (Tp1). Among the remaining precipitation events, those where each station had precipitation lasting less than 6 hours were classified as localized precipitation samples (Tp2). Considering the significant diurnal distribution of cloud water resources in the LM area (as detailed by Tian et al., 2019; Zhang et al., 2020; Xu et al., 2023), as well as the marked differences between night and afternoon cloud water resources (Xu et al., 2023), we focused on comparing and analyzing the hourly precipitation intensity during nighttime (20:00 to 06:00 the following day) and afternoon (12:00 to 19:00) periods influenced by four different types of airflow (see Figure 6)..

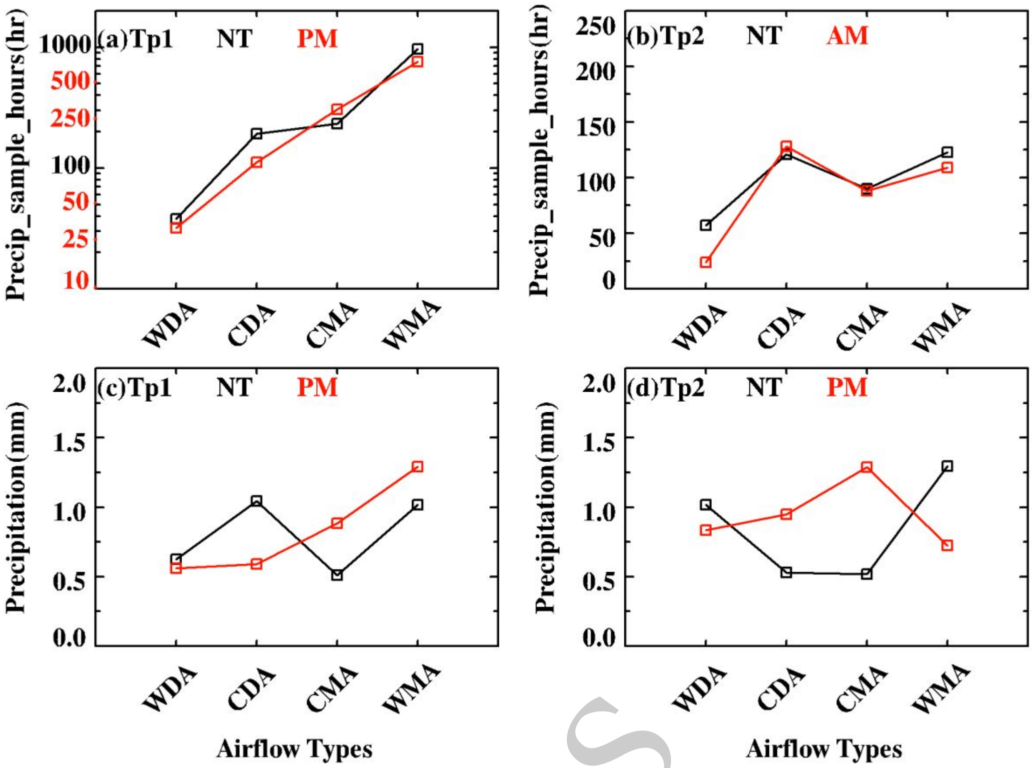

Figure 6 In LM during the rainy seasons (July to September) from 2020 to 2022 under different air mass transport pathways: (a) the sample size for regional precipitation, (b) the sample size for localized precipitation, (c) and (d) represent the average hourly precipitation for regional and localized precipitation events, respectively. The black dotted line and the red dotted line correspond to the nighttime and afternoon periods, respectively.

The amount and duration of precipitation under the influence of WMA and CMA are primarily concentrated in regional precipitation events, indicating that humid airflows are more likely to produce regional precipitation. For dry airflows, the duration and amount of regional precipitation are comparable to those of localized precipitation. With regard to regional precipitation (see Figure 6(c), the precipitation intensity generated by WMA during both the nighttime and afternoon periods is higher than that of the other three types of airflows, with average hourly precipitation values of 1.0

mm and 1.3 mm, respectively. It should be noted that the nighttime precipitation intensity under CDA is comparable to that of WMA, and is 1.8 times higher than during the afternoon period. This indicates that air temperature and humidity levels have complex effects on precipitation intensity. This might be due to the differing amplitudes of air temperature changes, dew point temperatures, and the height of lifting condensation level at night and in the afternoon for airflows with different properties of warmth and moisture.

For localized precipitation (see Figure 6(d)), the average hourly precipitation amount for cold airflows at night is 0.5 millimeters, which is only 45% of that for warm airflows. The situation is reversed during the afternoon, with cold airflows producing a greater precipitation intensity compared to warm airflows. This could be due to more intense convective activity in the afternoon compared to at night, as well as a more pronounced difference in temperature and humidity between the cold airflows and the surface transport air streams during the afternoon than at night. This difference is also more significant compared to airflows of other properties, leading to greater precipitation intensity from cold airflows during the afternoon period.

In summary, during regional precipitation events, WMA have a higher precipitation intensity both at night and in the afternoon compared to the other three types of airflows, while cold airflows show significant variations in precipitation intensity between nighttime and afternoon periods. During localized precipitation events, warm airflows produce higher precipitation intensity at night than cold airflows, but this trend reverses during the afternoon period.

3.3 The Mechanisms of Precipitation Influenced by Different Types of Airflows

Section 3.2 illustrates that precipitation intensity is closely related to the temperature and humidity characteristics of the transporting airflow. Moist air masses increase the release of latent heat in the rising air currents during the pseudo-adiabatic ascent process after saturation, thereby affecting the dynamic characteristics of the precipitation process. The underlying surface conditions, such as mountainous terrain, can also affect the stability of airflow, resulting in the vertical transport of water vapor. Hence, we examined the near-surface water vapor flux and unstable energy under the influence of airflows with different attributes. Moreover, we differentiated between the intensities of regional and localized precipitation. In accordance with the precipitation intensity gradation standards issued by the National Meteorological Administration (2012), precipitation exceeding 0.5mm per hour is defined as heavy precipitation, while precipitation of 0.3mm per hour or less is classified as light precipitation.

3.3.1 Regional Precipitation Mechanism

Part 3.2 indicates that under the influence of WMA, both the amount and intensity of precipitation are higher than those under three other types of air currents. This is closely related to the greater near-surface water vapor flux associated with this type of airflow, which has an average water vapor flux of 1.7 mm/min, compared to an approximately similar average of 1.4 mm/min for the other three types. Additionally, the water vapor flux from WMA during intense precipitation events is higher in the afternoon (1.9 mm/min) than at night (1.7 mm/min), consistent with the pattern of stronger precipitation in the afternoon compared to the nighttime under this type of airflow. On the other hand, Figure 7 (c) and (d) indicate that the unstable energy of WMA is approximately equal during both heavy and light precipitation events at different times of the day, suggesting that the main reason affecting the intensity of precipitation for this type of airflow is its level of moisture content. The direction of transport for this type of airflow aligns with terrain features that run approximately on a north-south axis, like an LP. Such terrain is conducive to the uplift of moisture-laden WMA, thereby causing more precipitation. The unstable energy is 2.0 and 1.8 J/(kg•m) at night and in the afternoon, respectively, both below that of the other three types of air currents during the same time frames, suggesting that the temperature difference between this type of airflow and the near-surface air is relatively small, resulting in relatively stable near-surface conditions. The distribution features of water vapor flux and unstable energy therefore indicate that the main reasons for the higher regional precipitation amounts and the stronger precipitation intensity with WMA are due to their higher water content when compared to the other three types of air currents, and that vertical transport of moisture has a limited impact on it.

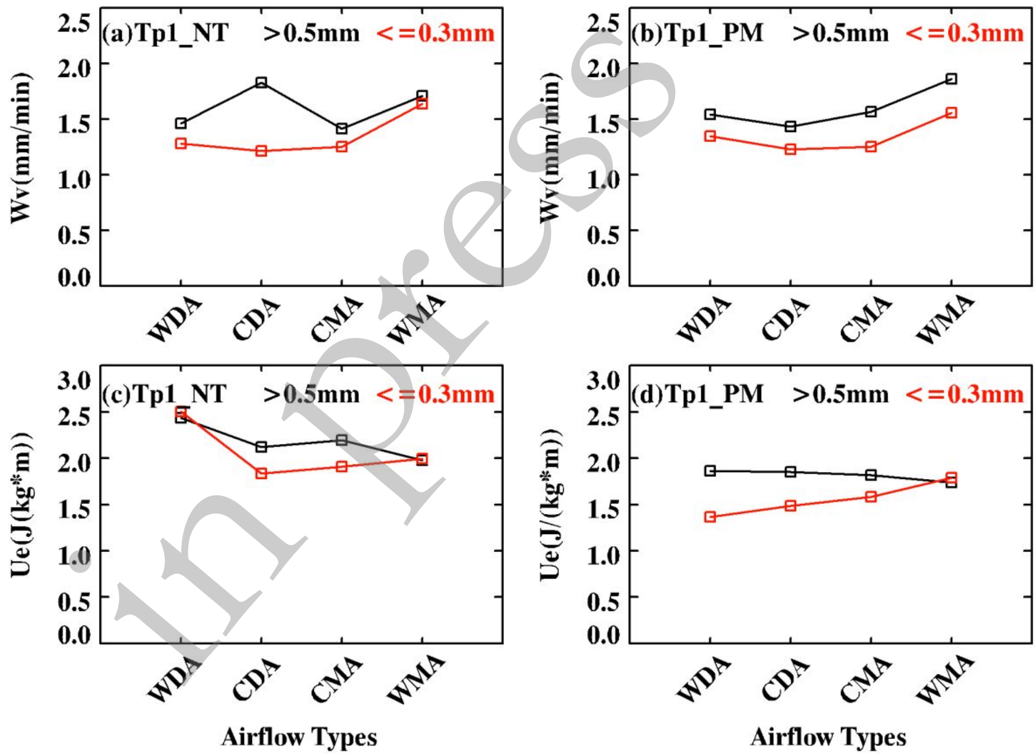

Figure 7 Near-surface water vapor flux and instability energy during regional precipitation events in the Liupan Mountains during the rainy seasons (July to September) from 2020 to 2022 influenced by different types of air mass transport, (a) nocturnal water vapor flux, (b) afternoon water vapor flux, (c) nocturnal instability energy, (d) afternoon instability energy. The black dotted

lines indicate intense precipitation events, while the red dotted lines indicate weak precipitation events.

The CMA exhibits stronger precipitation in the afternoon compared to nighttime, aligning with its average water vapor flux of 1.6 mm/min in the afternoon being higher than the nighttime average of 1.4 mm/min during heavy precipitation. Additionally, the pattern of higher unstable energy at night compared to the afternoon is consistent with that of the WMA. However, both the intensity of the precipitation and the water vapor flux values for CMA are less than those for WMA, indicating that CMA carry less moisture. The greater unstable energy of CMA at night may be related to the larger temperature differences caused by nocturnal radiative cooling near the ground, while the higher temperatures and greater evaporation during the afternoon period are the main reasons for the higher water vapor flux and, consequently, a greater precipitation intensity during this time. Under the influence of CMA, unstable energy is higher during intense precipitation events and lower during weak precipitation events as compared to WMA. This means that the stability of near-surface airflows varies greatly when it rains under CMA. This could be influenced on one hand by the significant temperature difference due to the lower temperatures of CMA compared to the warmer near-surface air, and on the other hand, by the meridional transport from the Qinghai-Tibet Plateau towards the east by CMA. As this airflow descends over the high-altitude regions in the west, momentum is transferred downwards, affecting the instability near the surface.

Dry airflows have a lower average water vapor flux compared to warm airflows, and carry less moisture content, which is consistent with their lower vapor fluxes. It is important to note that Figure 6(c) shows that the precipitation intensity of CDA at night is comparable to that of WMA. Similarly, in Figure 7(a), the water vapor flux during intense nighttime precipitation events for CDA is also on par with WMA. However, this characteristic does not extend to weak nighttime precipitation or to strong and weak precipitation processes during the afternoon. This could be due to the lower temperature and humidity of CDA compared to the other three types of airflows, creating a greater temperature-and-moisture gradient with the ground during the nighttime heavy precipitation events, leading to more unstable near-ground airflows and thereby enhancing vertical moisture transport. The precipitation intensity of CDA in the afternoon is similar to that of WDA and less than that of moist airflows, which is consistent with its water vapor flux being not much different from warm dry airflows but less than moist airflows. This suggests that the main factor influencing regional precipitation under different types of airflows is the degree of moisture enrichment.

During precipitation events, the near-surface water vapor flux values of WDA are not much different from those of CDA. What sets them apart from the other three types of airflows is that the values of unstable energy during both strong and weak nighttime precipitation, as well as during intense afternoon precipitation, are generally higher, with the unstable energy values during nighttime precipitation being significantly higher than the other three types of airflows, averaging 2.5 J/(kg•m). On the other hand, the difference in unstable energy between strong and weak afternoon precipitation is the greatest among the four types of airflows, while the difference in water vapor flux is smaller compared to moist airflows, indicating that thermodynamic and dynamic factors play a significant role in the precipitation process under WDA. The high unstable energy under WDA could be associated with the blocking effect of the steep terrain of the eastern LM. Gao (2020) pointed out in a simulation study of two precipitation cases over the LM that the terrain blocked the low-level easterly flows, causing airflow convergence and ascent on the eastern slope, thus enhancing precipitation on that side of the mountains.

In summary, water vapor content is the primary factor affecting the production of regional precipitation by airflows, with high moisture content in humid airflows being the main reason for their regional precipitation characteristics. Thermodynamic and dynamic factors are significantly reflected in the precipitation of dry airflows, with WDA having the least stability among the four types of airflow-related precipitation.

3.3.2 Localized precipitation mechanism

Localized precipitation is often closely associated with small-scale meteorological phenomena, such as local moisture convergence or the interaction of unstable energy causing upward motion. A comparison of localized and regional precipitation (see Figures 7 and 8) reveals that the near-surface water vapor flux and unstable energy changes during localized precipitation processes are more complex, which relates to the various factors that influence localized precipitation, such as local topography, surface conditions, atmospheric stability, and so on.

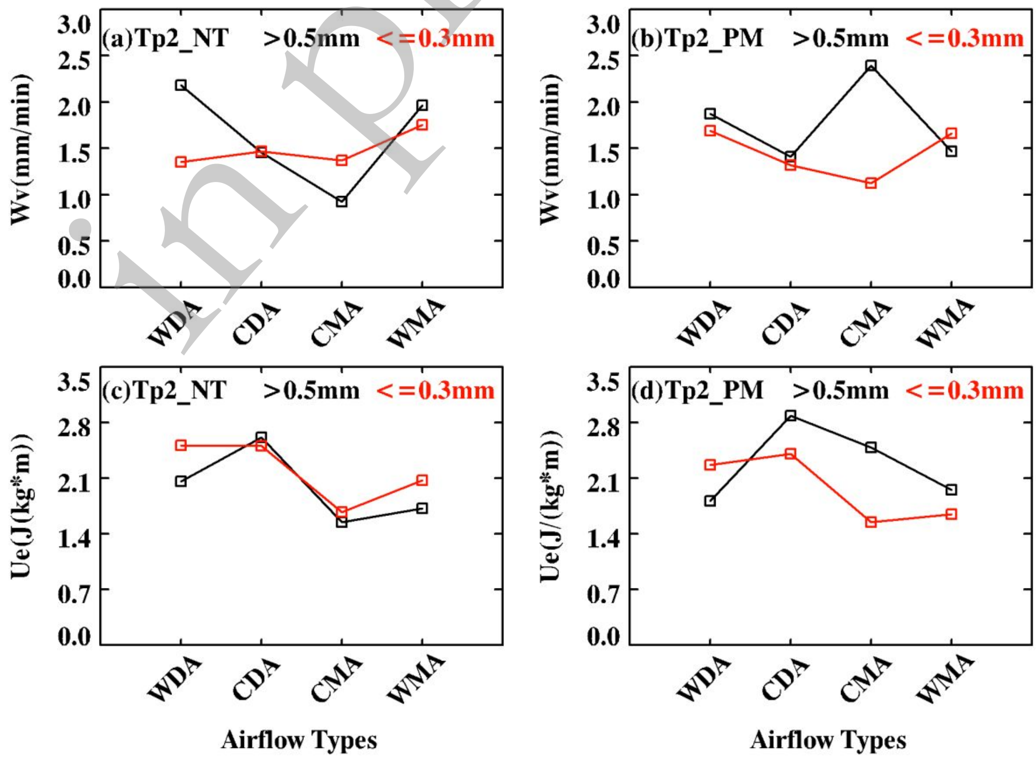

Figure 8 Near-surface water vapor flux and instability energy during localized precipitation events in the Liupan Mountains during the rainy seasons (July to September) from 2020 to 2022 under the influence of different types of air mass transport, (a) nocturnal water vapor flux, (b) afternoon water vapor flux, (c) nocturnal instability energy, (d) afternoon instability energy. The black dotted lines represent intense precipitation events, while the red dotted lines represent weak precipitation events.

As depicted in Figure 6(d), the intense nocturnal precipitation is primarily observed during heavy rainfall events with the WMA and WDA, which is consistent with the high moisture flux values during these events. The warm air flow is more dominant than the cold air flow, exceeding the regional precipitation by 15% and 50%, respectively. Compared to the WDA, the WMA has higher moisture flux but lower unstable energy, meaning that the WMA is more stable. However, due to its higher moisture content, it is capable of more vertical moisture transport. Although the WDA has relatively less moisture content, the more unstable stratification enhances the vertical transport of near-surface moisture, resulting in higher moisture flux. This indicates that the WDA is greatly influenced by local dynamic and thermodynamic factors during the localized precipitation process. The higher instability energy of the WDA, as compared to the WMA, is also associated with its interaction with the steep orographic barrier when transporting in the easterly direction, which causes the air flow to converge and rise, facilitating the vertical transport of more abundant near-surface moisture (Gao, 2020).

The unstable energy of the WDA during intense rainfall events is lower than that during weak rainfall events, indicating that dynamic factors produced by topographic influences play a significant role during the weak precipitation processes. In comparison with the similarly CDA, the WDA exhibits higher moisture flux and lower unstable energy during intense nocturnal precipitation and during both strong and weak precipitation in the afternoon. For warm air flows, their moisture carrying capacity is greater than that of cold air flows, not only because thermal conditions allow them to carry more moisture but also because they inherently contain more moisture, hence the higher moisture flux values of the WDA. On the other hand, the WDA has smaller temperature and humidity differences with the near-surface air flow compared to the CDA, resulting in smaller temperature and humidity gradients and consequently lower near-surface unstable energy than that of the CDA.

The weak nocturnal precipitation associated with the CMA aligns with its lower moisture flux. More specifically, during intense nocturnal rainfall, the moisture flux of the CMA decreases by 34% compared to regional precipitation, with an average unstable energy value of only 1.5 J(kg • m), the lowest among the four types of air flows. This suggests that at night, without the influence of major weather systems, the CMA has limited capacity for carrying moisture during localized precipitation processes. This is further evidenced by the small temperature differences with the near-surface layer at night, resulting in relative stability of the air flow and exhibiting characteristics of low moisture flux and low unstable energy. Additionally, the intensity of the CMA during intense afternoon rainfall exceeds the other three air flow types, consistent with its significantly higher moisture flux during this period. Compared to regional precipitation, its moisture flux increases by 53%, and unstable energy also increases by 37%. This might be due to the flow being colder and generating a larger temperature difference with the ground-heated air flow in the afternoon, enhancing the ground's thermal convection activity during this period. Furthermore, the air flow's trajectory toward the west is easily lifted by the topographic barrier of the LM running south to north, thus resulting in lower stability and intense vertical mixing of moisture. In conclusion, the variation in strength of localized precipitation associated with the CMA is consistent with changes in moisture flux and stability during intense precipitation, heavily influenced by thermodynamic and dynamic factors.

The CDA exhibits lower precipitation intensity at night, which is consistent with its lower moisture flux during intense rainfall events. This contrasts with regional precipitation, which has greater intensity and higher moisture flux values, indicating that under the influence of larger weather systems, the CDA has a higher moisture carrying capacity than under localized thermodynamic and dynamic conditions. The difference between regional and localized precipitation for the CDA is similar to that of the CMA. Moreover, the CDA has higher unstable energy than the other three air flow types during both strong and weak precipitation processes. In comparison with regional precipitation, unstable energy is 23% higher during intense rainfall and 37% higher during weak rainfall, with respective increases of 56% and 62% in the afternoon. This may be due to its low temperatures and low moisture content, which create larger humidity gradient differences when compared to the near-surface warm and moist air, leading to a more unstable atmosphere. On the other hand, the high unstable energy of the CDA might also be related to topographic influences. The flow's direction of transport and its approximation to the south-north orientation of the LM range promotes lifting of the near-surface warm moist air by the terrain, hence increasing the air flow's instability. In summary, during both night and afternoon periods, the CDA is characterized by low moisture flux and high unstable energy.

In summary, the variation of near-surface moisture flux and unstable energy during localized precipitation processes is more complex than in regional precipitation. Precipitation from different types of air flows is affected differently by their moisture content, differences in temperature and humidity characteristics, and thermodynamic and dynamic factors resulting from topographic influences.

4 Discussion

Mountainous terrain has a significant impact on the dynamic and thermodynamic processes of transporting airflows (Houze, 2012). On the windward slopes of mountains, airflow can be forced to lift, triggering convection (Seity et al., 2003), and can also cause blockage and accumulation of the transportation airflow. When the obstructed airflow is sufficiently moist, it can lead to the formation of clouds and precipitation (Neiman et al., 2002; Houze & Medina, 2005). The LM range generally extends in a north-south direction with a total length of about 240 kilometers, with steep eastern slopes and relatively gentle western slopes. Transporting airflows under different weather backgrounds will have complex interactions with the LM terrain, thereby affecting the precipitation processes in this region. As shown in Figure 9, the difference in regional precipitation sample size and average hourly precipitation between the east and western slopes under the influence of four types of airflows is not significant; however, there are larger differences during localized precipitation processes, with the disparity being more pronounced for dry airflows than for moist airflows.

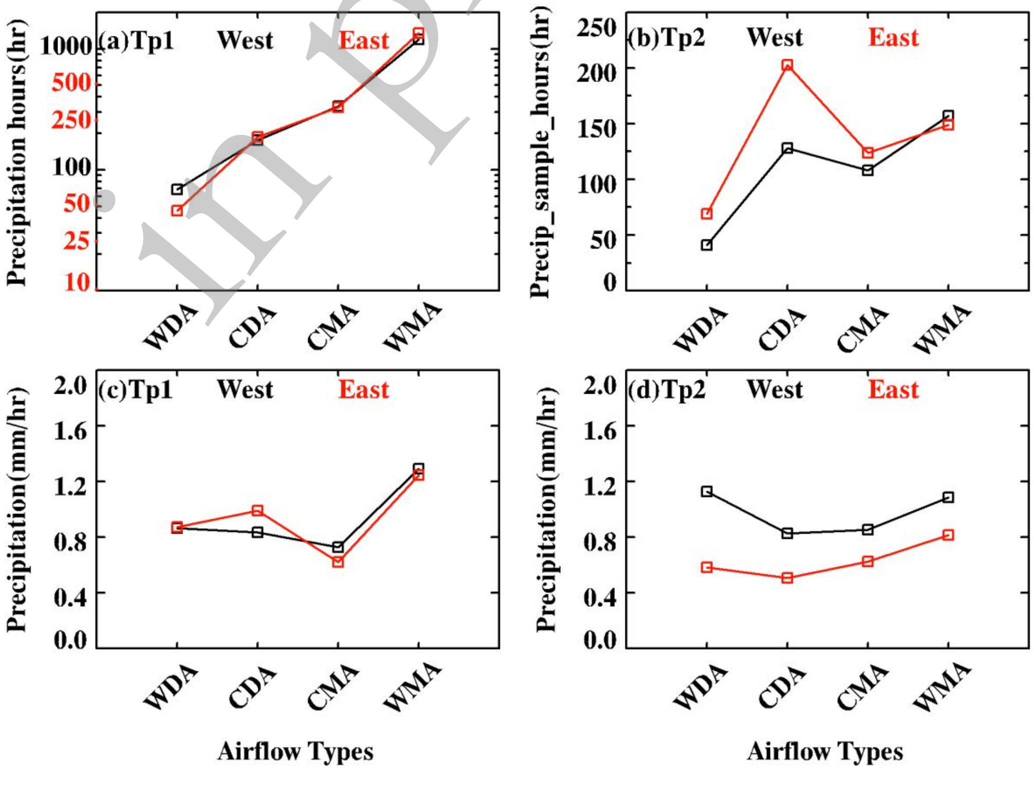

Figure 9 Comparison of precipitation intensity on the eastern and western slopes of the Liupan Mountains during the rainy seasons (July to September) from 2020 to 2022 under the influence of different types of airflows, (a) the sample size for regional precipitation events, (b) the sample size for localized precipitation events, (c) and (d) represent the average hourly precipitation for regional and localized precipitation events, respectively.

Airflow transport passing through mountainous terrain is subject to topographical influences, which induce alterations in the temperature and humidity distribution, and thus affect the precipitation process. During regional precipitation events, there is a characteristic pattern of higher near-surface moisture flux on the western slopes and lower on the eastern slopes, with unstable energy being lower on the western slopes and higher on the eastern slopes (as seen in Figure 10). This means that during precipitation on the eastern slopes, the near-surface airflow is more unstable and has less moisture content compared to the western slopes, which is related to the steeper terrain of the eastern slopes. Therefore, the airflow on the eastern slopes has stronger vertical dynamic transport, making it more prone to precipitation. On the other hand, under the influence of moist airflows, the differences in moisture flux and unstable energy between the eastern and western slopes are greater than those under dry airflows, which is the result of the combined influence of thermodynamic and dynamic processes due to the terrain. This indicates that terrain also has a significant effect on the regional precipitation process, but as seen in Figure 9(c), topography does not have a significant impact on regional precipitation intensity—the moisture content remains the main influencing factor.

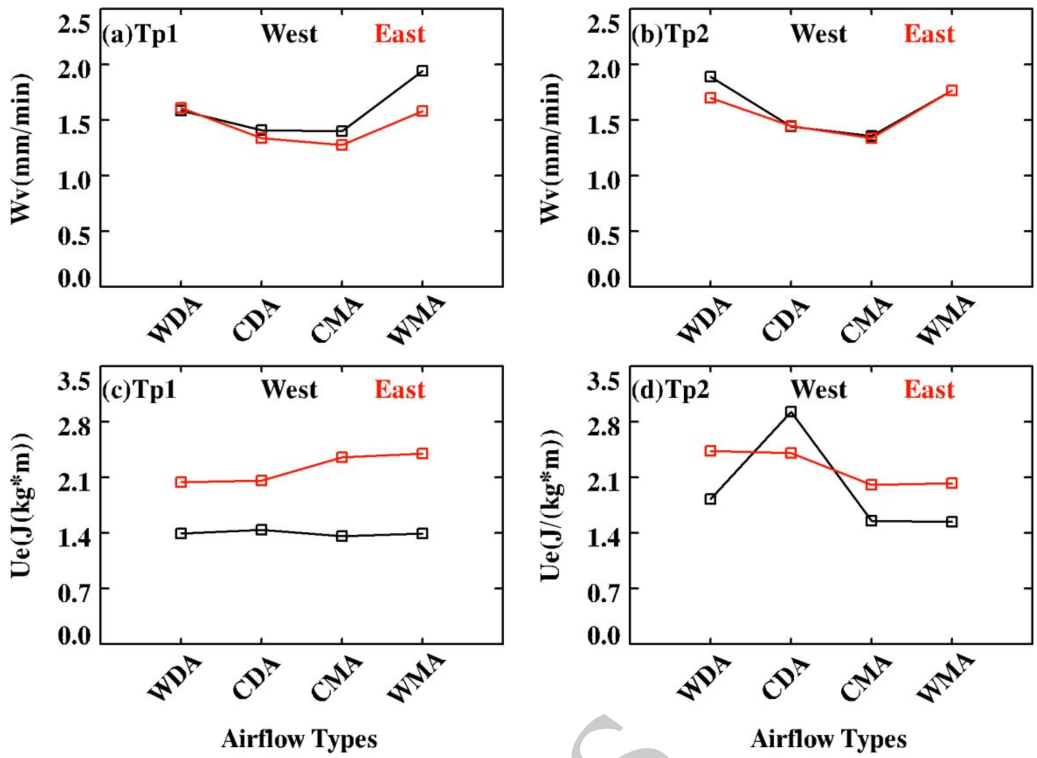

Figure 10 Comparison of precipitation intensity on the eastern and western slopes of the Liupan Mountains during the rainy season (July - September) from 2020 to 2022 under the influence of different types of airflows, (a) sample size of regional precipitation, (b) sample size of localized precipitation, (c) and (d) represent the average hourly precipitation of regional and localized precipitation, respectively.

When airflow encounters terrain, if buoyant instability occurs only within a shallow layer of air at low altitudes, terrain lifting may only trigger small cloud clusters on the windward side of the mountain. As small cloud clusters ascend along the slope, they may burst into small cumulonimbus clouds on the windward slopes. The difference in moisture flux between the eastern and western slopes during localized precipitation processes is relatively small, with the main difference reflected in unstable energy. Except for the CDA, where the unstable energy is higher on the western slope than on the eastern slope, the unstable energy for the other three types of airflows is higher on the eastern slope compared to the western slope. This is clearly related to the topographical differences between the eastern and western slopes, where the steep terrain of the eastern slope makes it more likely to precipitate than the western slope. This is evidenced by the greater number of precipitation hours on the eastern slope than on the western slope (as shown in Figure 9(b)), which also leads to a lower average hourly precipitation amount on the eastern slope compared to the western slope (as seen in Figure 9(d)). The higher unstable energy on the western slope under the influence of CDA may be related to the orientation of the LM range. The transport direction, which aligns with the LM orientation, facilitates the lifting of CDA by the terrain. Moreover, the temperature and humidity gradients of this type of airflow are more significant compared to the other three types, making it subject to more notable dynamic and thermodynamic influences, resulting in greater instability of the airflow. In conclusion, mountainous terrain has a significant impact on localized precipitation processes.

5. Conclusions and summary

The article utilizes three years of cumulative observational data from the LM gradient station since its establishment, combined with backward trajectory clustering analysis of transport airflows, to study the precipitation characteristics and their influencing mechanisms under different types of airflows during the rainy season in LM. The main conclusions are summarized as follows.

（1）Rainy and overcast weather in LM is mainly influenced by the transport of CMA and WMA. The cumulative hours of overcast and rainy weather under the transport of CMA and WMA are 1.5 and 2.2 times that of clear weather, respectively, while the cumulative hours of clear weather under CDA and WDA transport are 1.3 and 1.1 times that of overcast and rainy weather. The precipitation amounts from WMA, CMA, WDA and CDA transport paths account for 68%, 12%, 10%, and 9.8% of the total precipitation, respectively.

（2）The intensity of precipitation from WMA is higher during nighttime and afternoon periods than the other three types of airflows, while precipitation from WDA is relatively weak. The intensity variation of the four types of airflows during localized precipitation events is more significant than in regional precipitation. The intensity of precipitation from cold airflows at night is only 45% of that from warm airflows, but during the afternoon, precipitation from cold airflows is actually stronger than from warm airflows.

（3）The primary reason for the distinctive regional precipitation characteristics of WMA is their higher water content compared to the other three types of airflows, with the stability of the airflow having a minor influence. The precipitation characteristics of CMA are not only affected by the moisture content but also more evidently influenced by thermodynamic and dynamic factors compared to warm, moist airflows. Thermodynamic and dynamic factors have a more significant impact on regional precipitation from dry-leaning airflows than from those that are moisture-leaning.

（4）In localized precipitation, moisture content is the main factor influencing the precipitation characteristics of WMA. Thermodynamic and dynamic factors significantly affect both CMA and dry airflows. This is particularly evident in the strong precipitation events occurring in the afternoon with CMA and the weak precipitation processes associated with WDA. The stability of CDA during precipitation processes is generally weak.

（5）Terrain has varying degrees of influence on the regional and localized precipitation produced by the four types of airflows, with a more significant impact on localized precipitation than on regional precipitation.

Acknowledgments. We appreciate the data provided by the Key Laboratory of Monitoring, Early Warning and Risk Management of Agricultural Meteorological Disasters with Special Characteristics in Dry Areas of the China Meteorological Administration (CMA) and the Key

Laboratory of Meteorological Disaster Prevention and Mitigation in Ningxia, ERA5 data provided by ECMWF (https://cds.climate.copernicus.eu), the GDAS data provided by NOAA (https://www.ready.noaa.gov/archives.php). The work was supported by the National Natural Sciences Foundation of China (42075073, 42075077).

REFERENCES

Banta, R. M., 1990: The role of mountain flows in making cloud. *Meteorological Monographs*, 23(45): 229-283.

Barros, A. P., and Lettenmaier, D. P., 1994: Dynamic modeling of orographically induced precipitation. *Reviews of geophysics*, 32(3): 265-284.

Chen, Y., Huang, J., Wang, T., Jin, H., Ge, J., 2005:Temporal and spatial distribution of the different clouds over northwestern China with the relation to precipitation. *Journal of Applied Meteorological Science (in Chinese)*, 16(6):717-727+862.

Cheng, G., and Wang, G., 2006: Changing trend of drought and drought disaster in northwest China and counter measures. *Earth Science Frontiers (in Chinese)*, 13(1):3-14. DOI:10.3321/j.issn:1005-2321.2006.01.002.

Deng, P., Sang, J., Yang, M., Mu, J., Chang, Z., Cao, N., 2021: Analysis of difference characteristics of precipitation and air water vapor conditions over east and west slopes of Liupan Mountain in recent 30 years. *Mete. Sci. Tech.*, 49(1):77-85. DOI:10.19517/j.1671-6345.20200061.

Feng, L., and Zhou, T., 2012: Water vapor transport for summer precipitation over the Tibetan Plateau: Multidata set analysis, *J. Geophys. Res.*, 117, D20114, doi:10.1029/2011JD017012.

Gao, L., 2020: Numerical study on orographic summertime cloud structure and precipitation mechanism over the Liupan Mountain area [D]. *Chinese Academy of Meteorological Sciences*, 19-21. DOI:10.27631/d.cnki.gzqky.2020.000041

General Administration of Quality Supervision, Inspection and Quarantine of PRC, & Standardization

Administration of PRC. (2012). GB/T 28592-2012: Grading of precipitation. Beijing: Standards Press of China.

Giovannettone, J. P., and Barros, A. P., 2009: Probing Regional Orographic Controls of Precipitation and Cloudiness. *Journal of Hydrometeorology*, 10(1):167-182.

Gui, J., Li, Z., Feng, Q., Zhang, B., Xue, J., Gao, W., Li, Y., Liang, P., and Nan, F., 2022: Water resources significance of moisture recycling in the transition zone between Tibetan Plateau and arid region by stable isotope tracing. *Journal of Hydrology*, 605: 127350.

Houze, R. A., 2012: Orographic effects on precipitating clouds. *Rev. Geophys.*, 50(1):1-47. RG1001. DOI:10.1029/2011rg000365.

Houze, R. A., and Medina, S., 2005: Turbulence as a Mechanism for Orographic Precipitation Enhancement. *J. Atmos. Sci.*, 62, 3599-3623. https://doi.org/10.1175/JAS3555.1.

Huang, R. H., Liu, Y., Du, Z. C., Chen, J. L. and Huang, J. L., 2017: Differences and links between the East Asian and South Asian summer monsoon systems: Characteristics and variability. *Adv. Atmos. Sci.*, 34(10): 1204-1218, doi: 10.1007/ s00376-017-7008-3.

Huang, R., and Chen, J., 2010: Characteristics of the summertime water vapor transports over the eastern part of China and those over the western part of China and their difference. *Chinese Journal of Atmospheric Sciences (in Chinese)*, 34(06):1035-1045.

Li, Y., Zhang, C., and Wang, Y., 2016: The verification of millennial-scale monsoon water vapor transport channel in northwest China. *Journal of Hydrology*, 536: 273-283.

Li, Z., Gao, Y., Wang, Y., Pan, Y., Li, J., Chen, A., Wang, T., Han, C., Song, Y., and Theakstone, W.H., 2015: Can monsoon moisture arrive in the Qilian Mountains in summer?. *Quaternary international*, 358: 113-125.

Liu, Y, Chang, S., Hua, S., and Huang, J., 2018: A review of the research on atmospheric water resources over arid and semi-arid regions of East Asia. *Acta Meteorologica Sinica (in Chinese)*, 76(03):485-492.

Neiman, P. J., Ralph, F. M., White, A. B., and Kingsmaill, D., 2002: The Statistical Relationship between Upslope Flow and Rainfall in California's Coastal Mountains: Observations during CALJET. *Mon Weather Rev.*, 130(6):1468-1492. DOI:10.1175/1520-0493(2002)1302.0.CO;2.

Qi, P., Guo, X., Chang, Y., Tang, J., and Li, S., 2022: Cloud water path, precipitation amount, and precipitation efficiency derived from multiple datasets on the Qilian Mountains, Northeastern Tibetan Plateau. *Atmospheric Research*, 274: 106204.

Scholl, M. A., Giambelluca, T., W., Gingerich, S., B., Nullet, M.,A., and Loope, L., L., 2007: Cloud water in windward and leeward mountain forests: The stable isotope signature of orographic cloud water. *Water Resources Research*, 43(12):1-13.

Seity, Y., Soula, S., Tabary, P., and Scialom, G., 2003: The convective storm system during IOP 2a of MAP: Cloud-to-ground lightning flash production in relation to dynamics and microphysics, *Q. J. R. Meteorol. Soc.*, 129: 523-542, doi:10.1256/ qj.02.03.

Sevruk, B., and Nevenic, M., 1998: The geography and topography effects on the areal pattern of precipitation in a small prealpine basin. *Water Science and Technology*, 37(11): 163-170.

Simmonds, I., Bi, D., and Hope, P., 1999: Atmospheric water vapor flux and its association with rainfall overchina in summer. *Journal of Climate*, 12(5): 1353-1367.

Tao, S. Chen, Y., and L. X., 1987: A review of recent research on the East Asian summer monsoon in China [M]//Chang C P, Krishnamurti T N. Monsoon Meteorology. *Oxford: Oxford University Press*, 60-92.

Tian Lei, Sang Jianren, Yao Zhanyu, Chang Zhuolin, Dan Xinlan, Cao Ning, Sun Yanqiao, 2019: Characteristics of atmosphereic water vapor and liquid water in Liupan Mountain area in summer and autumn. *Journal of Meteorology and Environment*, 35(6): 28-37.

Wang, G., Li, T., Li, J., Wei, J., and Zhong, D., 2016: Analysis of sky water resources in the source region and the upper-middle region of the Yellow River basin. *Yellow River (in Chinese)*, 38(10):79-82. DOI:10.3969/j.issn.1000-1379.2016.10.016.

Wang, K., Jiang, H., and Zhao, H., 2005: Atmospheric water vapor transport from westerly and monsoon over the Northwest China. *Advances in Water Science (in Chinese)*, 16(3):432-438. DOI:10.3321/j.issn:1001-6791.2005.03.021.

Wang, X., Pang, G., Yang, M., Wan, Guoning, and Liu, Z., 2018: Precipitation changes in the Qilian Mountains associated with the shifts of regional atmospheric water vapour during 1960–2014. *International Journal of Climatology*, 38(12): 4355-4368.

Xu, K., Zhong, L., Ma, Y., Zou, M., and Huang, Z., 2020: A study on the water vapor transport trend and water vapor source of the Tibetan Plateau. *Theoretical and Applied Climatology*, 140: 1031-1042.

Xu, R., and Qiu, Y., 2023: The Difference in Cloud Water Resources and Precipitation on the Eastern and Western Sides of the Liupan Mountains Caused by Topographic Effects. *Atmosphere*, 14: 1502. https://doi.org/10.3390/ atmos14101502.

Zhang, P., Yao, Z., Jia, S., Chang, Z., Sang, J., Gao, L., Zhao, W., Wang, W., and Zhu, X., 2020: Study of the Characteristics of Atmospheric Water Resources and Hydrometeor Precipitation Efficiency over the Liupan Shan Area. *Chinese Journal of Atmospheric Sciences (in Chinese)*, 44(2): 421-434. doi:10.3878/j.issn.1006-9895.1904.19104

Zhang, Q., Zhang, J., Sun, G., and Di X., 2008: Research on water-vapor distribution in the air over Qilian Mountains. *Acta Meteorologica Sinica English edition*, 22(1): 107.

Zhou, T. J., and Yu, R. C., 2005: Atmospheric water vapor transport associated with typical anomalous summer rainfall patterns in China. *J. Geophys. Res.*, 110, D08104, doi:10.1029/2004JD005413.